Inelastic analysis of octagonal concrete-filled steel tubular short columns under eccentric loading

Received: 9 May 2023 | Revised: 2 September 2023 | Accepted: 18 October 2023

DOI: 10.1002/suco.202300360

ARTICLE

fib CEB-FIP WILEY

Inelastic analysis of octagonal concrete-filled steel tubular short columns under eccentric loading

Mizan Ahmed[1] | **Qing Quan Liang**[2] | **Vipulkumar Ishvarbhai Patel**[3] | **Ahmed Hamoda**[4]

[1]Centre for Infrastructure Monitoring and Protection, School of Civil and Mechanical Engineering, Curtin University, Bentley, Western Australia, Australia

[2]College of Sport, Health, and Engineering, Victoria University, Melbourne, Victoria, Australia

[3]School of Computing, Engineering and Mathematical Sciences, La Trobe University, Bendigo, Victoria, Australia

[4]Civil Engineering Department, Faculty of Engineering, Kafrelsheikh University, Kafrelsheikh, Egypt

Correspondence
Qing Quan Liang, College of Sport, Health, and Engineering, Victoria University, PO Box 14428, Melbourne, VIC 8001, Australia.
Email: qing.liang@vu.edu.au

Abstract

Octagonal concrete-filled steel tubular (OCFST) columns combine the benefits of circular and square concrete-filled steel tubular (CFST) columns so that they not only possess higher strength and ductility but also provide the ease of connection to composite beams. However, research studies have been very limited on the performance analysis of OCFST short beam-columns subjected to eccentric loading. In this study, a fiber-based numerical model is developed for the performance simulation of high-strength OCFST short beam-columns under eccentric loading. The simulation model takes into account material nonlinearities and concrete confinement induced by the octagonal steel tube. Computational methods are given that predict the axial load–moment interaction curves and moment–curvature responses of OCFST beam-columns. The developed fiber model is verified against available test data with good accuracy. The influences of important parameters on the responses of high-strength OCFST short beam-columns are studied by means of utilizing the computational model. It is found that the behavior of OCFST beam-columns is significantly influenced by the diameter-to-thickness ratio of the cross-section, concrete strength, steel yield stress, and axial load ratio. Interaction equations are proposed for expressing the axial load–moment strength envelopes of the cross-sections of OCFST beam-columns and validated against numerical results.

KEYWORDS

axial load–moment interaction, concrete-filled steel tubes, fiber element modeling, moment-curvature response, octagonal columns

1 | INTRODUCTION

Concrete-filled steel tubular (CFST) beam-columns exhibit high stiffness, strength, and ductility owing to the interaction of the steel and concrete components. These beam-columns are often used as bridge piers and in super large structures to carry heavy loads.[1–3] A circular CFST column has higher concrete confinement than its square and rectangular counterpart as pointed out by Sakino et al.[4] However, the connections of steel beams to a

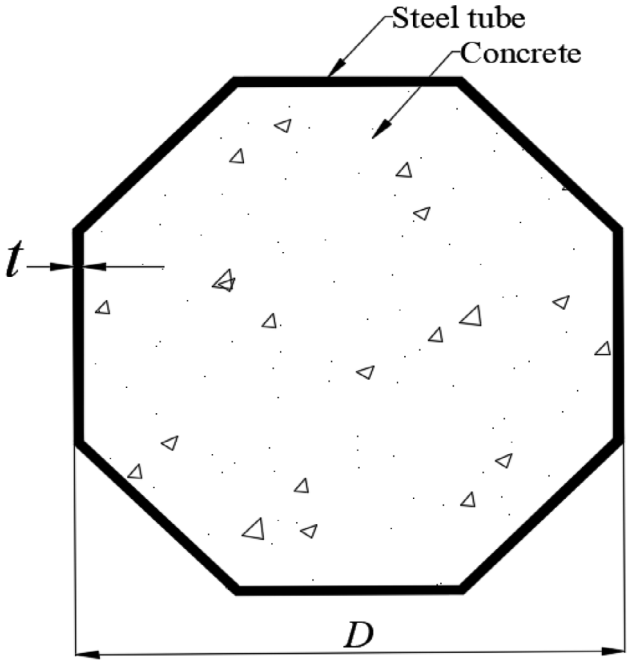

FIGURE 1 Cross-section of OCFST beam-column. OCFST, octagonal concrete-filled steel tubular.

rectangular CFST column can be constructed with ease, which makes rectangular CFST columns the most favorable choice in practical design. To carry the same ultimate axial load of the circular CFST column, the cross-section of the square CFST column needs to be increased. Recently, octagonal CFST (OCFST) columns as depicted in Figure 1 have been considered as an improved version of CFST columns as they combine the advantages of both square and circular CFST columns. The octagonal steel tube provides greater confinement to the core concrete and is less susceptible to local buckling than the square one. In addition, an octagonal steel tube has flat walls, which can be easily connected with steel beams in a composite frame.

Although there has been significant research undertaken on circular and square CFST columns,[4–10] there is little published information on the characteristics of OCFST beam-columns loaded eccentrically. Test results presented by researchers[11–17] showed that the strengths and ductility of octagonal cross-sections are higher than those of square sections.

Fang et al.[17] reported the first investigation into the structural behavior of OCFST short beam-columns loaded eccentrically. Twelve OCFST beam-columns were tested to examine the effects of diameter-to-thickness (D/t) ratio and loading eccentricities on their structural behavior. These column specimens were constructed using 104 MPa concrete and 758 MPa steel. The ductile failure was observed when the OCFST short beam-columns were loaded eccentrically. Moreover, it was reported that the increase in loading eccentricity significantly reduced the ultimate strengths of OCFST columns.[17]

The numerical simulations of OCFST short columns under axial compression were performed by Ding et al.,[13] Fang et al.,[17] Susantha et al.,[18] Hassanein et al.,[19] and Ahmed and Liang.[20] Ahmed and Liang[20] developed a new concrete confinement model for axially loaded OCFST columns. The confinement model of Ahmed and Liang[20] provided a more accurate estimation of the performance of OCFST columns than those by other researchers. No design equations were given in Eurocode 4[21] and AISC 360-16[22] for determining the ultimate axial strength of OCFST columns loaded axially. Therefore, Ahmed and Liang[20] proposed a simplified equation for assessing the ultimate axial strength of OCFST short columns. The applicability of the current design rules for circular and square CFST columns to OCFST short columns under axial compression has been assessed by Ahmed and Liang.[20] They concluded that Eurocode 4[21] significantly overestimated the ultimate strengths of OCFST columns while AISC 360-16[22] provided conservative prediction of their ultimate strengths.

Fang et al.[17] developed a finite element (FE) model using ABAQUS for the simulation of the structural performance of eccentrically loaded OCFST short columns. Their model can predict the load–moment diagram by increasing the loading eccentricity; however, it cannot predict the pure bending moment capacity. Furthermore, Fang et al.[17] utilized the methods specified in Eurocode 4[21] and AISC 360-16[22] to determine the load–moment interaction curves of OCFST beam-column. Eurocode 4 and AISC 360-16 suggest that the confinement effect should be considered in the strength calculations of circular CFST columns, but it can be neglected in that of square ones. Fang et al.[17] ignored the confinement effect on the ultimate strengths of OCFST columns. However, it is obvious that the cross-section of OCFST column is close to that of a circular tube, thereby providing considerable confinement to the core concrete.

This study fills a gap in the research on OCFST short beam-columns that are eccentrically loaded. A fiber element model is developed, which efficiently determines the inelastic behavior of the cross-section of an OCFST short beam-column subjected to eccentric loading. The simulation procedures are given for obtaining the load–moment interaction diagrams and moment–curvature curves of OCFST beam-columns. The accuracy of the fiber-based computer model is evaluated by comparison with experimental results given by Fang et al.[17] The verified computer model is employed to parametrically study the moment–curvature responses and axial load–moment

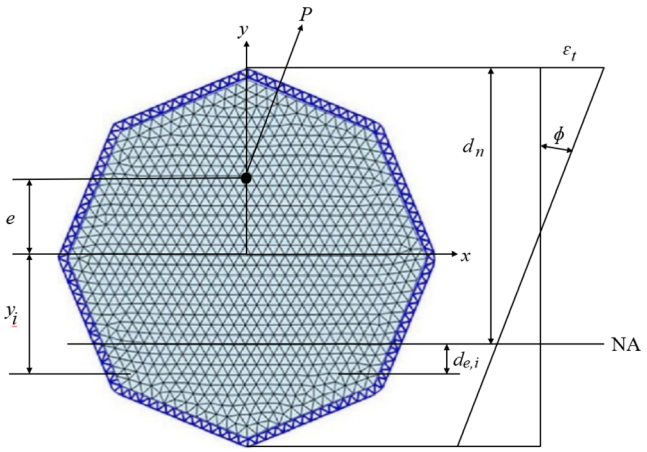

FIGURE 2 Discretization of the cross-section of OCFST beam-column. OCFST, octagonal concrete-filled steel tubular.

interaction behavior of OCFST beam-columns. Design equations are given that express the load–moment interaction curves of OCFST beam-columns. The proposed equations as well as the design approaches specified in AISC 360-16[22] for CFST columns are assessed for their applicability to OCFST beam-columns.

2 | FORMULATION OF THE FIBER-BASED NUMERICAL MODEL

2.1 | Basic concepts of fiber analysis

The ultimate strength of a beam-column with a slenderness L/r ratio less than 22 is governed by its cross-sectional strength, as specified in AS 3600-2009.[23] The fiber-based numerical model is an efficient computational tool for the performance simulation of composite columns.[24,25] In the FE analysis of an OCFST column, the column along its length must be divided into FEs which contain many degrees of freedom. On the contrary, the fiber-based numerical model does not require the discretization of the column along its length and does not employ complicated contact elements to model the interaction of steel and concrete components. Therefore, the fiber model is computationally more efficient than the FE model while maintaining good accuracy as reported by Ahmed et al.[26] In the fiber method of analysis, the cross-section of an OCFST column is discretized into small fiber elements as presented in Figure 2. For this purpose, a mesh discretization technique given by Persson and Strang[27] is adopted. The algorithm for fiber discretization was designed based on simple mechanical analogy where the nodal locations are solved for equilibrium in 2-D truss structures using the linear force–displacement relationship and the topology is reset by the Delaunay algorithm.[27] The number of fibers in the cross-section depends on the edge length specified by the user. A smaller edge length results in finer resolution for the fibers as shown in Figure 2. Each fiber is assigned to the constitutive laws of either structural steel or concrete. The plane section is assumed to remain plane after bending, resulting in a linear strain distribution through the depth of the cross-section as shown in Figure 2.[7] This assumption was also made in the fiber analysis by other researchers.[28–30] In addition, it is assumed that the bond between the steel and the concrete in the longitudinal direction is perfect. For any given curvature, the strain in each fiber element is obtained from the linear strain profile, so that the stress can be determined from the stress–strain relationships.[7,31] Equations (1) and (2) are then utilized to compute the internal axial load (P) and moment (M) in the cross-section of an OCFST beam-column under eccentric loading.

$$P = \sum_{i=1}^{ns} \sigma_{s,i} A_{s,i} + \sum_{j=1}^{nc} \sigma_{c,j} A_{c,j}, \tag{1}$$

$$M = \sum_{i=1}^{ns} \sigma_{s,i} A_{s,i} y_i + \sum_{j=1}^{nc} \sigma_{c,j} A_{c,j} y_j, \tag{2}$$

in which M and P denote the internal bending moment about the x-axis and internal axial force, respectively; $\sigma_{s,i}$ stands for the longitudinal steel stress of steel fiber i, $\sigma_{c,j}$ represents the longitudinal concrete stress of concrete fiber j, $A_{s,i}$ denotes the steel element area of fiber i, $A_{c,j}$ denotes the concrete element area of concrete fiber j, y_i represents the coordinate at centroid of steel fiber i, ns stands for the total steel fibers, nc represents the total concrete fibers, and y_j denotes the coordinator at the centroid of concrete fiber j.

2.2 | Moment-curvature analysis

The moment-curvature analysis is used to determine the bending strength of the cross-section. In the analysis, for a specified axial load, the bending curvature is gradually increased. The internal axial force of the cross-section under the given curvature is obtained from Equation (1) and compared with the applied axial load for equilibrium. The neutral axis depth (d_n) is iteratively adjusted to satisfy the force equilibrium condition by using the inverse quadratic solution method proposed by Ahmed et al.[32] The internal moment for each curvature increment is then calculated. The complete $M-\phi$ curve is obtained by repeating the computational process until the moment (M) drops to 50% of the maximum moment

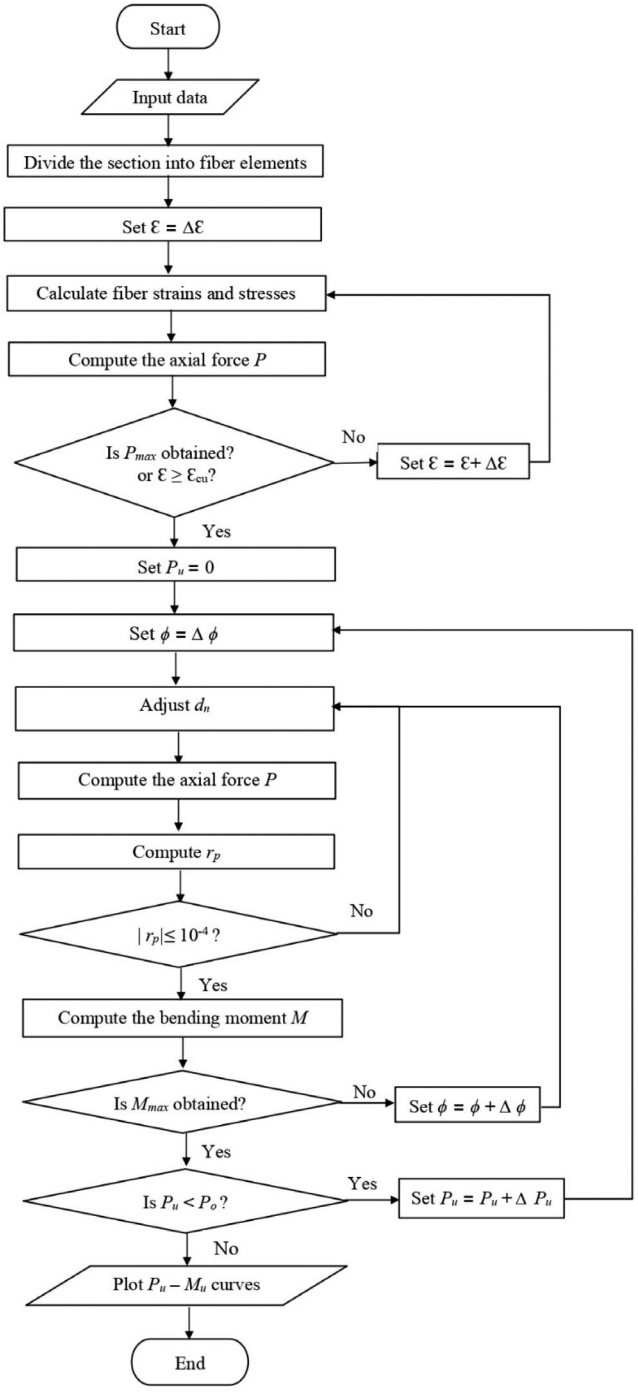

FIGURE 3 Flowchart to calculate the P_u-M_u curves of OCFST columns. OCFST, octagonal concrete-filled steel tubular.

(M_{max}) or the concrete compressive strain exceeds the maximum strain (ε_{cu}), specified as 0.04.

2.3 | Axial load–moment interaction analysis

To develop the P_u-M_u interaction diagram, the section ultimate axial load (P_o) of the OCFST column under axial compression is firstly computed using the procedure given by Ahmed and Liang.[20] The axial load is then increased from 0 to P_o with a step of $P_o/10$. For each load step, the corresponding ultimate moment is calculated by using the $M-\phi$ simulation program described in Section 2.2. The analysis process is repeated until the last load step has been executed. The proposed analysis procedure results in a set of axial loads and section moment capacities that are used to plot the P_u-M_u curve. Figure 3 illustrates the flowchart for calculating the P_u-M_u curves of OCFST beam-columns.

2.4 | Curvature ductility index

The curvature ductility index proposed by Liang[7] is utilized to calculate the flexural ductility of an OCFST beam-column, which is expressed as

$$\mathrm{PI}_{cd}=\frac{\phi_u}{\phi_y}, \tag{3}$$

where ϕ_y denotes the yield curvature, which is determined as $\phi_{0.75}/0.75$, where $\phi_{0.75}$ is the curvature when the moment attains 75% of the ultimate moment capacity.[7] In Equation (3), ϕ_u is the ultimate curvature of the section. For the descending moment–curvature response, ϕ_u is taken as the curvature when the moment drops to 90% of the ultimate moment capacity.

3 | MATERIAL CONSTITUTIVE MODELS

3.1 | Stress–strain relationship of steel

The material behavior of steel tube is simulated by its uniaxial stress–strain relationships. The adopted stress–strain relation is suitable for mild steel, cold-formed steel, and high-strength steel. The curve is identical in both compression and tension. Generally, mild structural steel shows a typical yield plateau, which can be simulated using the trilinear stress–strain curve shown in Figure 4.[7] For the cold-formed steel, the stress–strain curve is proposed as rounded, whereas for the high-strength steel, the rounded part of the cold-formed steel is replaced with a straight line,[7] as illustrated in Figure 4. The rounded part of the stress–strain curve is mathematically expressed by

$$\sigma_s=f_{sy}\left(\frac{\varepsilon_s-0.9\varepsilon_{sy}}{\varepsilon_{st}-0.9\varepsilon_{sy}}\right)^{1/45}\quad\left(0.9\varepsilon_{sy}<\varepsilon_s\le\varepsilon_{st}\right). \tag{4}$$

Equation (4) was proposed by Liang.[7] In Equation (4), σ_s denotes the stress of the steel elements, ε_s denotes the

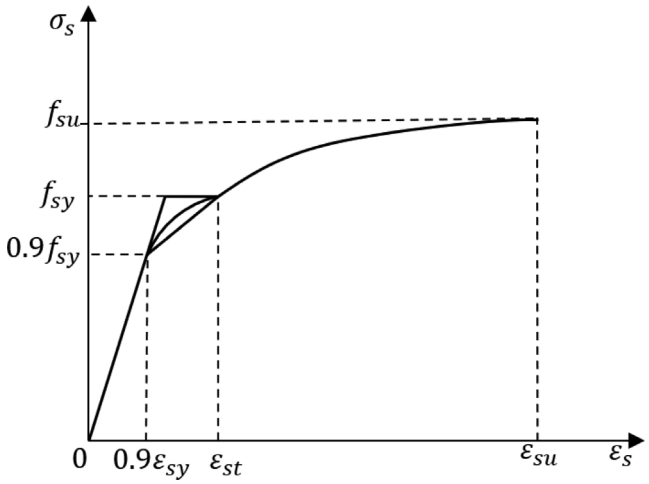

FIGURE 4 Stress–strain relations for steels in tension and compression.

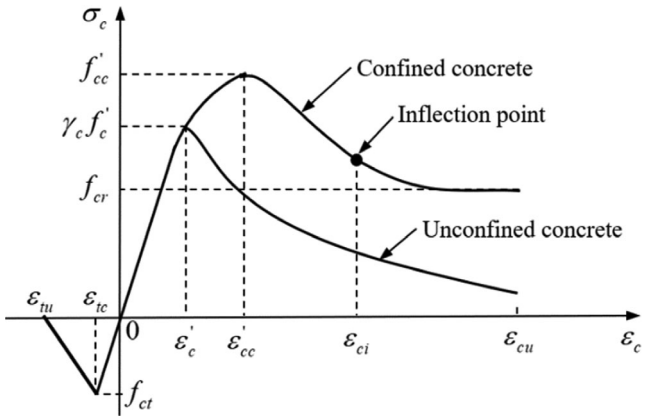

FIGURE 5 Stress–strain relationships for concrete in compression and tension.

strain of the steel fiber, f_{sy} and ε_{sy} represent the steel yield strength and strain, respectively, and ε_{st} denotes the strain hardening strain, which is equal to 0.005. In Figure 4, f_{su} represents the steel tensile strength and ε_{su} denotes the ultimate strain. The stress–strain relation in Figure 4 accounts for the effect of biaxial stresses on the steel tube of the OCFST column owing to the confinement mechanism by decreasing the yield strength of steel by 10%.[4,28] For the strain beyond the strain hardening strain ε_{st}, the stress of the steel is obtained from the equations proposed by Mander[33] until the ultimate strain ε_{su} is attained. The ultimate strain value of steel ε_{su} is specified as 0.2.

3.2 | Stress–strain relationship of concrete

The nonlinear stress–strain relation adopted for the concrete applies to both high-strength and normal-strength concrete $\left(20\text{MPa} \le f'_c \le 100\text{MPa}\right)$. The stress–strain relation of concrete accounts for the confinement effect, which increases both the ductility and strength of the concrete. As the strength increases, the stress–strain relation features an increase in the strain at the ultimate strength. However, the higher the concrete strength, the more brittle the behavior and the lower concrete confinement. The stress–strain relations of confined and unconfined concrete demonstrated in Figure 5 only apply to short-term quasi-static loading. The compressive strength of unconfined concrete is represented using the cube strength f_{cu} or the strength of the standard concrete cylinder f'_c. It is assumed that the ratio of the cube strength f_{cu} to the cylinder strength f'_c is 0.85. The initial modulus of elasticity E_c in both compression and tension follows the equation proposed by Lim and Ozbakkaloglu.[34]

$$E_c\ (\text{MPa}) = 4400\sqrt{\gamma_c f'_c}, \tag{5}$$

where γ_c is the reduction factor recognizing the column size effects calculated using the expression given by Liang.[7] The reduction factor is calculated as $\gamma_c = 1.85D_c^{-0.135}$, in which D_c is calculated as $D-2t$, where D is the external largest width of the octagonal section and t is the thickness of the steel tube. The strain at the maximum stress for confined concrete ε'_{cc} is given in Equation (6), which was originally reported by Popovics.[35]

$$\varepsilon'_{cc} = \varepsilon'_c + \frac{k_2 f_{rp}\varepsilon'_c}{\gamma_c f'_c}. \tag{6}$$

The maximum strain of the unconfined concrete was suggested by De Nicolo et al.[36] as

$$\varepsilon'_c = 0.00076 + \sqrt{\left(0.626\gamma_c f'_c - 4.33\right)\times 10^{-7}}. \tag{7}$$

The ultimate compressive strength f'_{cc} of the confined concrete is determined by the formula originally reported by Popovics[35] as

$$f'_{cc} = \left(1 + \frac{k_1 f_{rp}}{\gamma_c f'_c}\right)\left(\gamma_c f'_c\right), \tag{8}$$

where f_{rp} is the confining pressure to the core concrete; k_1 and k_2 are equal to 4.1 and 20.5, respectively.[37] The value of factors k_1 and k_2 are given by Richart et al.[38] The confinement in OCFST column is different from that

in conventional circular and square CFST columns. Based on the test data of OCFST columns under axial load, Ahmed and Liang[20] proposed Equation (9) to express the lateral pressure f_{rp} on the filled concrete in OCFST columns.

$$f_{rp}\ (\text{MPa}) = 3.1963 - 6.8835 \times 10^{-3}\left(\frac{D}{t}\right) \quad \left(f_{rp} \geq 0\right). \quad (9)$$

The stress–strain relationship originally reported by Popovics[35] is adopted to represent the material behavior of concrete in ascending branch in compression and expressed by

$$\sigma_c = \frac{f'_{cc}\left(\varepsilon_c/\varepsilon'_{cc}\right)\lambda}{\left(\varepsilon_c/\varepsilon'_{cc}\right)^{\lambda} + \lambda - 1}, \quad \text{for} \quad 0 \leq \varepsilon_c \leq \varepsilon'_{cc}, \quad (10)$$

$$\lambda = \frac{E_c\varepsilon'_{cc}}{E_c\varepsilon'_{cc} - f'_{cc}}, \quad (11)$$

where σ_c is the concrete stress and ε_c is the corresponding strain at σ_c. The post-peak branch of the stress–strain relationship of confined concrete is obtained by using the equation developed by Lim and Ozbakkaloglu[34] as

$$\sigma_c = f'_{cc} - \frac{f'_{cc} - f_{cr}}{1 + \left(\frac{\varepsilon_c - \varepsilon'_{cc}}{\varepsilon_{ci} - \varepsilon'_{cc}}\right)^{-2}}, \quad \text{for} \quad \varepsilon_c > \varepsilon'_{cc}, \quad (12)$$

in which f_{cr} represents the residual strength of confined concrete, taken as $f_{cr} = \beta_c f'_{cc}$, where β_c stands for the strength degradation parameter and ε_{ci} denotes the inflection strain taken as 0.01.[20] The expression of β_c proposed by Ahmed and Liang[20] is

$$\beta_c = 1.145243 - 0.003898\left(\frac{D}{t}\right) - 0.005853\left(\gamma_c f'_c\right) \quad (0 \leq \beta_c \leq 1). \quad (13)$$

The stress–strain relationship for concrete in tension is illustrated in Figure 5 where the tensile stress and strain are taken as negative. It can be seen from Figure 5 that the linear relationship between tensile stress and strain is assumed for concrete before and after cracking. The tensile strength of concrete is estimated as $f_{ct} = 0.6\sqrt{\gamma_c f'_c}$ while the maximum tensile strain ε_{tu} is taken as $\varepsilon_{tu} = 10\varepsilon_{tc}$, where ε_{tc} is the cracking strain.

4 | VERIFICATION OF THE NUMERICAL MODEL

In this section, the accuracy of the fiber simulation model is verified by comparing the predicted axial load–strain curves, strength envelopes, and load–deflection curves of OCFST short beam-columns with experimental measurements.

4.1 | The axial load–strain curves of OCFST short columns under axial loading

The predicted axial load–strain curves of OCFST short columns under axial loading are compared against the test results reported by Ding et al.[13] and Zhu and Chan.[15] From Figure 6, it is seen that the numerical model can accurately predict the axial load–strain curves of OCFST short columns.

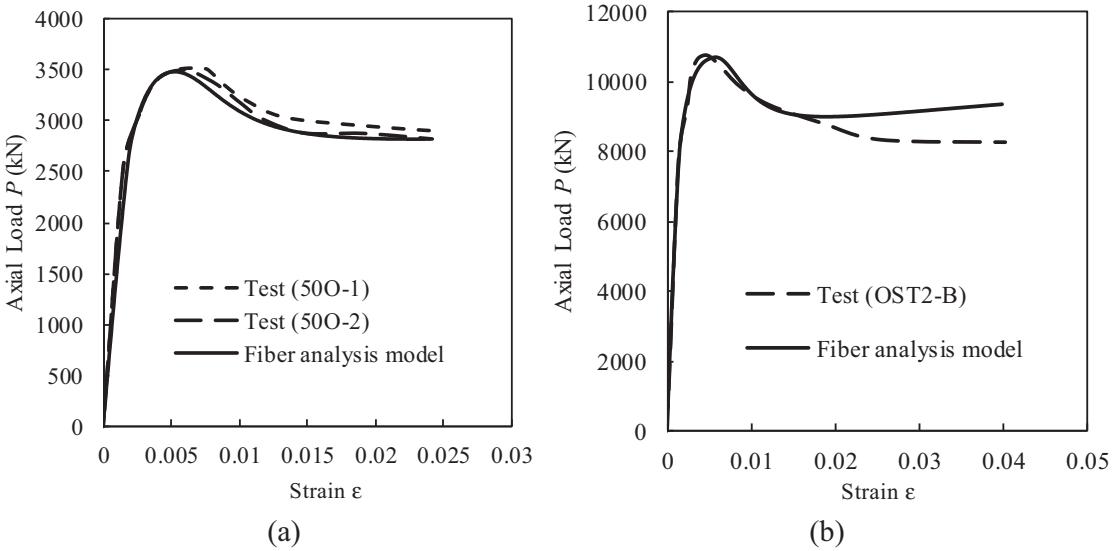

FIGURE 6 Comparison of predicted and experimental axial load–strain curves of OCFST short columns tested by (a) Zhu and Chan[15] and (b) Ding et al.[13] OCFST, octagonal concrete-filled steel tubular.

TABLE 1 Dimensions and material properties of OCFST beam-columns.

Column	D (mm)	t (mm)	D/t	f_{sy} (MPa)	f'_c (MPa)	e (mm)	$P_{u,exp}$ (kN)	$M_{u,exp}$ (kNm)	Ref.
Oct-50 × 6-e10	121	6.1	19.8	758	104.2	10.8	2641	28.52	Fang et al.[17]
Oct-50 × 6-e20	121	6.1	19.8	758	104.2	20.3	2184	44.34	
Oct-50 × 6-e40	121	6.1	19.8	758	104.2	40.4	1593	64.36	
Oct-50 × 6-e60	121	6.1	19.8	758	104.2	59.9	1191	71.34	
Oct-50 × 6-e75	121	6.1	19.8	758	104.2	76.1	996	75.80	
Oct-50 × 6-e90	121	6.1	19.8	758	104.2	90.1	866	78.03	
Oct-70 × 6-e20	169	6	28.2	758	104.2	20.8	3209	66.75	
Oct-70 × 6-e35	169	6	28.2	758	104.2	35.5	2837	100.71	
Oct-70 × 6-e60	169	6	28.2	758	104.2	60.1	1975	118.70	
Oct-70 × 6-e60R	169	6	28.2	758	104.2	60.9	1946	118.51	
Oct-70 × 6-e75	169	6	28.2	758	104.2	75.6	1895	143.26	
Oct-70 × 6-e90	169	6	28.2	758	104.2	91.2	1532	139.72	

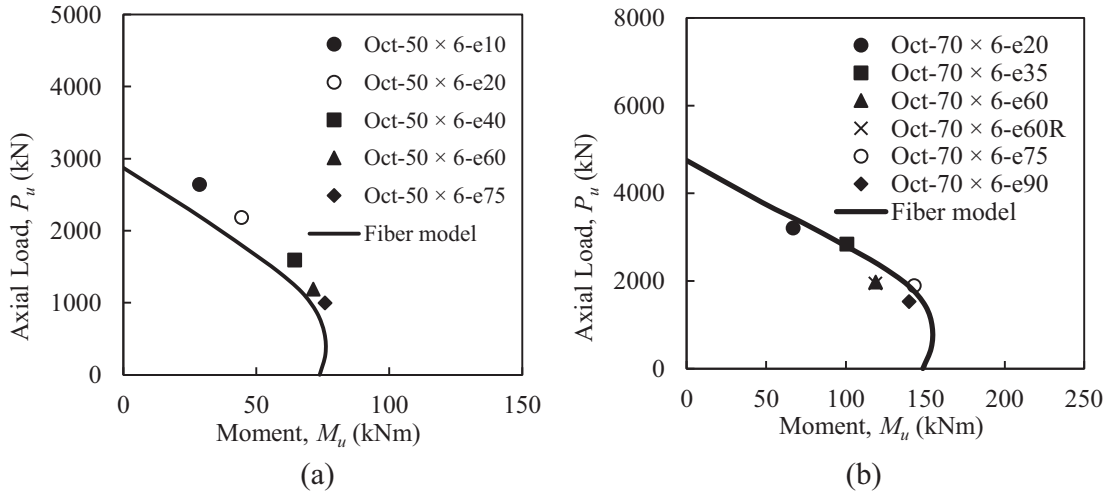

FIGURE 7 Comparison of predicted and measured $P_u - M_u$ curves of OCFST columns. OCFST, octagonal concrete-filled steel tubular.

4.2 | Load–moment interaction curves of OCFST beam-columns

The predicted load–moment interaction curves of OCFST beam-columns are compared with the experimental results given by Fang et al.[17] The basic column parameters of the tested specimens are displayed in Table 1. In Table 1, the first specimen is designated as Oct-50 × 6-e10, where 50 is the nominal edge length (mm), 6 stands for the thickness of the tube (mm), and e10 refers to the loading eccentricity (e) of 10 mm. The ultimate moment $M_{u,exp}$ was calculated as $M_{u,exp} = P_{u,exp} \times e$, where $P_{u,exp}$ is the experimental ultimate load. It can be seen from Figure 7 that the fiber modeling technique can capture the $P_u - M_u$ diagrams of OCFST columns with reasonable accuracy. The small discrepancies between predictions and measurements are likely caused by the uncertainty in the material properties of concrete and steel, systematic errors in scientific measurements, and gross errors in experimental techniques. Moreover, the strength enhancements due to cold-forming, reduction in strength due to welding, and ignoring the corner effect may cause some discrepancies between the test and numerical predictions.

4.3 | Load–deflection curves

The modeling and simulation method proposed by Ahmed et al.[32,39] has been implemented into the present numerical model to determine the axial load–lateral deflection curves. The numerical model has been

employed to predict the axial load–lateral deflection ($P-u_m$) curves of OCFST short columns tested by Fang et al.[17] The results obtained are presented in Figure 8. A reasonable match between the test and numerical prediction can be observed.

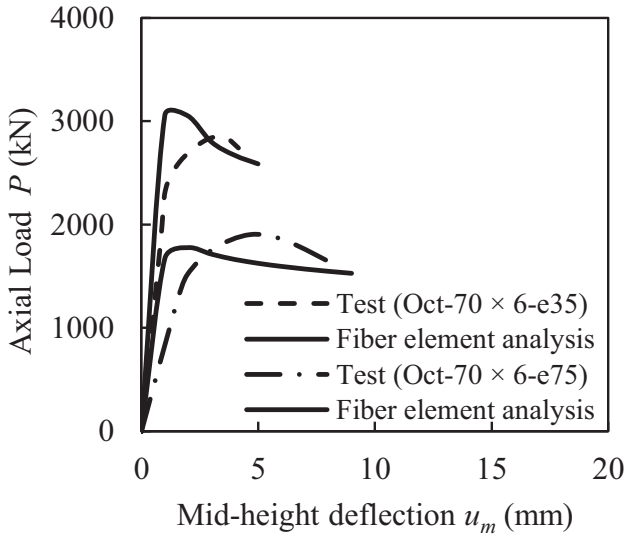

FIGURE 8 Comparison of predicted and measured $P-u_m$ curves of OCFST columns. OCFST, octagonal concrete-filled steel tubular.

5 | PARAMETRIC STUDY

The fiber-based model was employed to assess the influences of various parameters on the behavior of eccentrically compressed OCFST short beam-columns. The external diameter of the OCFST columns was taken as 700 mm with a steel tube thickness of 10 mm. The concrete strength was 70 MPa. The steel yield strength was 350 MPa; Young's modulus of steel was 200 GPa. The axial load ratio (P_u/P_o) was 0.4. Table 2 summarizes the geometry and material properties of OCFST beam-columns utilized in the parametric study.

5.1 | Influences of D/t ratio

The influences of D/t on the structural characteristics of OCFST short beam-columns were studied by employing the fiber modeling technique. The D/t ratios of 50–80 were determined by varying external diameter (Group G1) or the tube thickness (Group G2). Figure 9 shows that increasing the D/t ratio by increasing the external diameter of the columns (Group G1) significantly enlarges the P_u-M_u diagram of the columns. This is due to the increase in the cross-sectional area of the confined concrete when the D/t ratio increases by increasing the

TABLE 2 Details of the reference beam-columns utilized in the parametric study.

Group	Column	D (mm)	t (mm)	D/t	f_{sy} (MPa)	f'_c (MPa)	P_u/P_o
G1	OCFST-1	500	10	50	350	70	0.4
	OCFST-2	600	10	60	350	70	0.4
	OCFST-3	700	10	70	350	70	0.4
	OCFST-4	800	10	80	350	70	0.4
G2	OCFST-5	700	14	50	350	70	0.4
	OCFST-6	700	11.66	60	350	70	0.4
	OCFST-7	700	10	70	350	70	0.4
	OCFST-8	700	8.75	80	350	70	0.4
G3	OCFST-9	700	10	70	250	70	0.4
	OCFST-10	700	10	70	350	70	0.4
	OCFST-11	700	10	70	460	70	0.4
	OCFST-12	700	10	70	650	70	0.4
G4	OCFST-13	700	10	70	350	30	0.4
	OCFST-14	700	10	70	350	50	0.4
	OCFST-15	700	10	70	350	70	0.4
	OCFST-16	700	10	70	350	100	0.4
G5	OCFST-17	700	10	70	350	70	0.4
	OCFST-18	700	10	70	350	70	0.5
	OCFST-19	700	10	70	350	70	0.6
	OCFST-20	700	10	70	350	70	0.7

external diameter of the columns. As demonstrated in Figure 9, the pure moment capacity also increases with an increase in the D/t ratio of the columns. Furthermore, it is found that increasing D/t ratio remarkably increases the ultimate moment and ductility of the columns, as illustrated in Figure 10. The ultimate moment of the columns is found to increase by 219.5% when increasing the D/t ratio from 50 to 80. The residual moment at the ultimate curvature of the columns with D/t ratio of 50, 60, 70, and 80 is 55%, 63%, 81%, and 81% of their ultimate moment, respectively. The ductility of the column improves from 3.25 to 6.27 as the D/t ratio increases from 50 to 80. These numerical results suggest that OCFST short beam-columns with a larger D should be used to resist heavy loads.

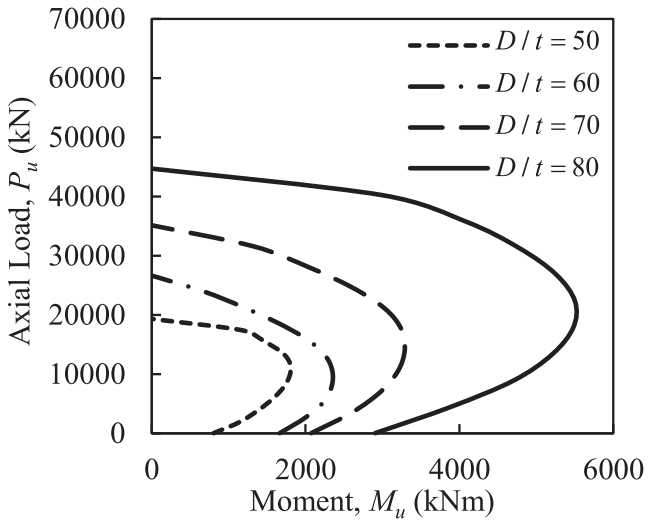

FIGURE 9 Influences of D/t ratio on the $P_u - M_u$ curves by changing the external diameter of the columns.

On the other hand, increasing the D/t ratio by changing the tube thickness (Group G2) has significant effects on the $P_u - M_u$ and $M - \phi$ curves as well as on the ductility of the columns, as shown in Figures 11 and 12. When the D/t ratio of the column increases from 50 to 80, the ultimate moment of the column decreases by 23.6%. Similarly, the ductility of the column reduces from 7.88 to 4.93 as the D/t ratio increases from 50 to 80. This is because increasing the D/t ratio by reducing the tube thickness reduces the steel area of the columns, thereby reducing the moment capacity of the columns. Figure 12a demonstrates that the initial flexural stiffness of OCFST short beam-columns decreases with increasing the D/t ratio.

5.2 | Influences of steel yield strength

The fiber-based model of nonlinear analysis was employed to predict the influences of steel yield strength on the structural performance of OCFST short beam-columns. The steel yield strength was changed from 250 to 650 MPa for the columns in Group G3. From the results shown in Figure 13, it is observed that the $P_u - M_u$ diagram is enlarged by increasing the steel yield stress. The steel yield strength has the most pronounced effect on the ultimate pure moment capacity of the cross-section of OCFST beam-columns. This implies that high-strength steel tubes can be utilized to construct OCFST beam-columns to resist large bending moments. As depicted in Figure 14a, the initial flexural stiffness is not affected by the value of steel yield strength. However, the ultimate moment capacity of OCFST short beam-columns is considerably increased by using higher strength steel. What

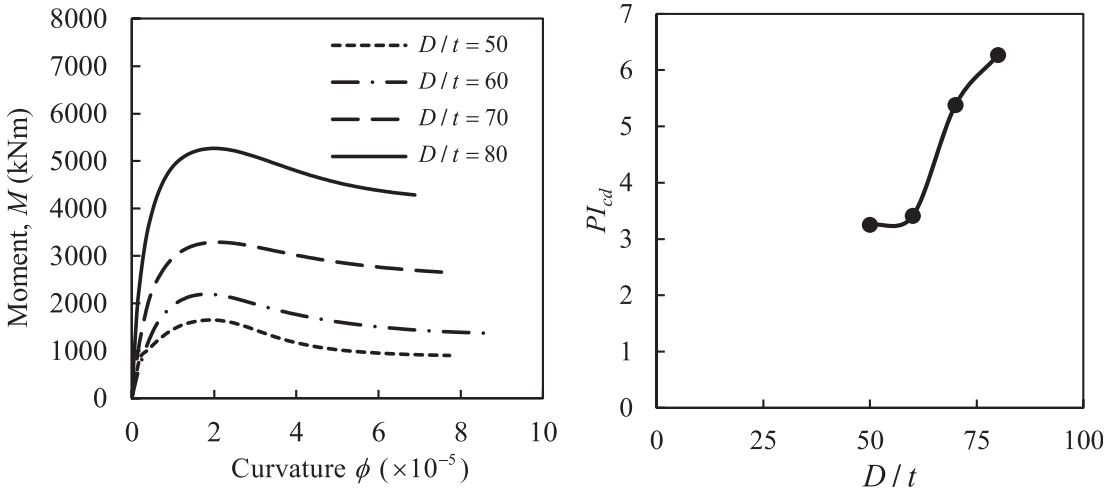

(a) $M - \phi$ curves (b) Curvature ductility

FIGURE 10 Influences of D/t ratio (changing D only) on the strength and ductility. (a) $M - \phi$ curves. (b) Curvature ductility.

stands out in this figure is that changing the steel yield strength from 250 to 650 MPa improves the ultimate moment capacity by 41.3%. The steel yield stress has an insignificant influence on the ductility of the columns as can be seen in Figure 14b. The ductility indices of the columns with steel yield stresses of 250, 350, 460, and 550 MPa are 5.32, 5.38, 5.36, and 5.73, respectively.

5.3 | Influences of concrete compressive strength

The influence of the concrete compressive strength on the behavior of octagonal CFST beam-columns was studied by varying the strength of the columns in Group G4 from 30 to 100 MPa. From the load–moment diagram in Figure 15, it is apparent that increasing the concrete compressive strength enlarges the $P_u - M_u$ curves of OCFST columns. The most interesting aspect of these $P_u - M_u$ diagrams in Figure 15 is that increasing the concrete compressive strength results in a greater increase in the pure ultimate axial strength rather than the pure ultimate moment capacity. This effect on the ultimate axial strength reduces as the bending moment increases. This is consistent with the performance of other composite short beam-columns.[40,41] This suggests that high strength concrete can be utilized in OCFST beam-columns to resist concentric compression force rather than bending moments. As Figure 16a depicts, increasing concrete strength from 30 to 100 MPa increases the ultimate moment of the columns by 99.1%. However, the ductility of the column is found to reduce from 5.59 to 5.15 as the concrete strength increases from 30 to 100 MPa. This result is explained by the fact that high-strength concrete is brittle at the material level. The flexural stiffness of OCFST beam-columns increases as the concrete compressive strength increases (Figure 16a). This is because Young's modulus of concrete increases with the increase in the compressive strength.

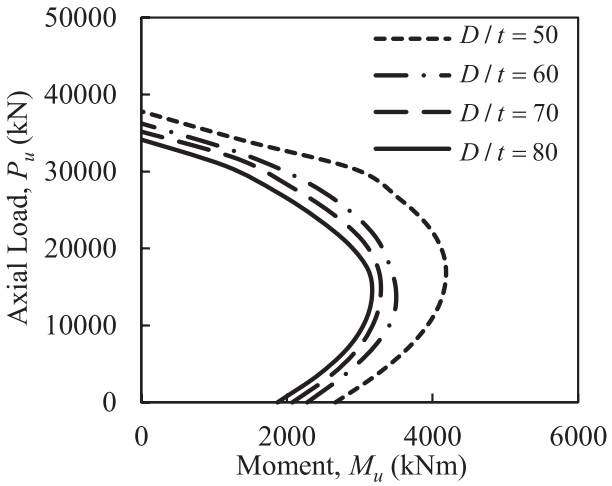

FIGURE 11 Influences of D/t ratio by changing steel tube thickness on the $P_u - M_u$ curves of OCFST columns.

5.4 | Influences of the axial load ratio

The axial load level is represented by the P_u/P_o ratio. The computer model was utilized to investigate the

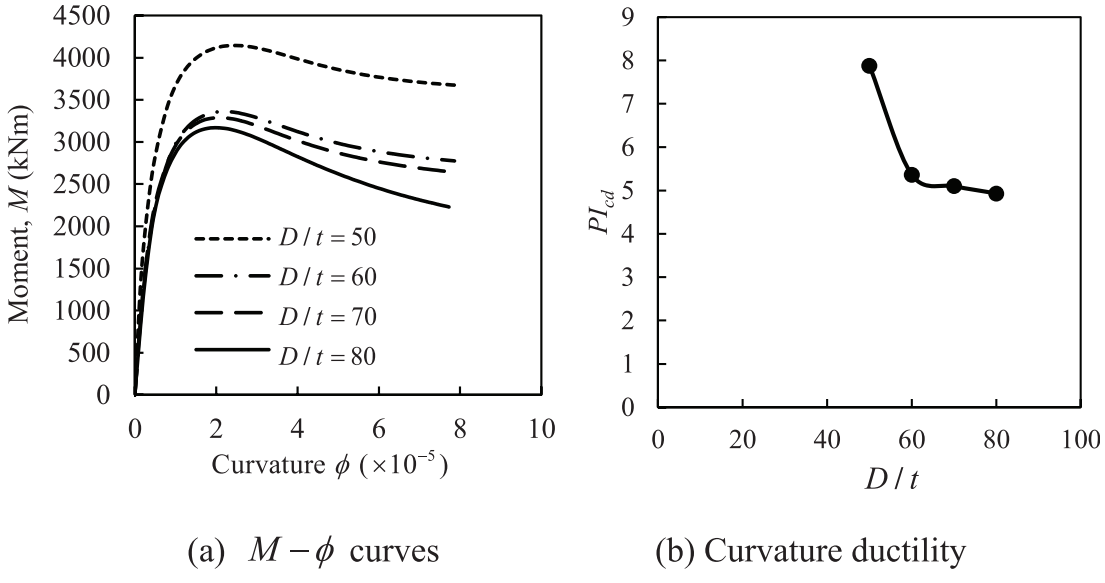

FIGURE 12 Influences of D/t ratio by changing the steel tube thickness on the behavior of OCFST columns. (a) $M-\phi$ curves. (b) Curvature ductility. OCFST, octagonal concrete-filled steel tubular.

influence of the P_u/P_o ratio on the behavior of OCFST beam-columns given in Group G5 by changing the P_u/P_o ratio from 0.4 to 0.7. Figure 17a presents the effects of P_u/P_o ratio on the moment–curvature responses. The figure reveals that increasing P_u/P_o ratio significantly reduces the flexural stiffness, ultimate moment, and curvature ductility of the columns. The ultimate moment of the column reduces by 16.1% when the axial load level increases from 0.4 to 0.7. Similarly, the flexural ductility of the column reduces from 5.38 to 2.63 as the axial load level increases from 0.4 to 0.7.

6 | INTERACTION EQUATIONS OF OCFST SHORT COLUMNS

6.1 | AISC 360-16

The expressions for the axial load–moment interaction diagrams of CFST columns given in AISC 360-16[22] are

$$\begin{aligned} &\frac{P_u}{P_o}+\frac{8M_u}{9M_o}=1 \quad \text{for} \quad \frac{P_u}{P_o}\geq 0.2 \\ &\frac{P_u}{2P_o}+\frac{M_u}{M_o}=1 \quad \text{for} \quad \frac{P_u}{P_o}<0.2 \end{aligned}, \tag{14}$$

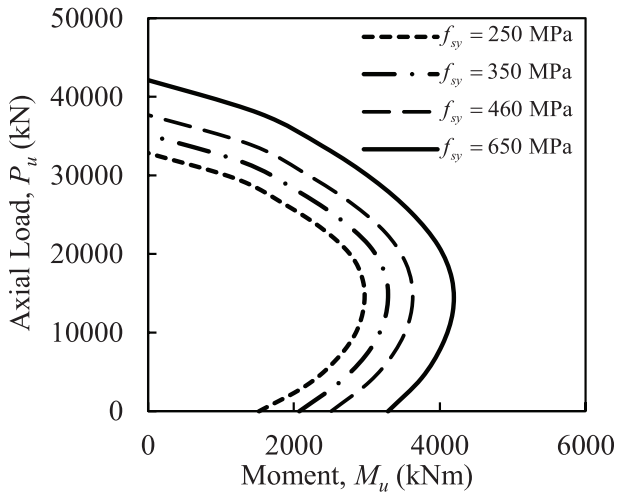

FIGURE 13 Influences of steel yield stress on P_u-M_u curves of octagonal CFST beam-columns. CFST, concrete-filled steel tubular.

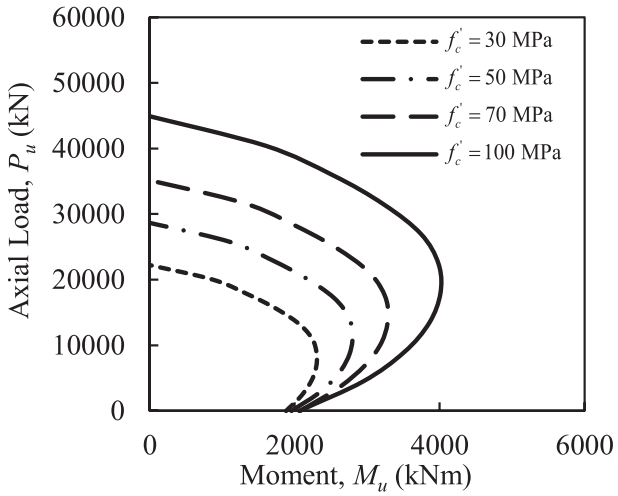

FIGURE 15 Influences of concrete strength on P_u-M_u diagram of OCFST beam-columns. OCFST, octagonal concrete-filled steel tubular.

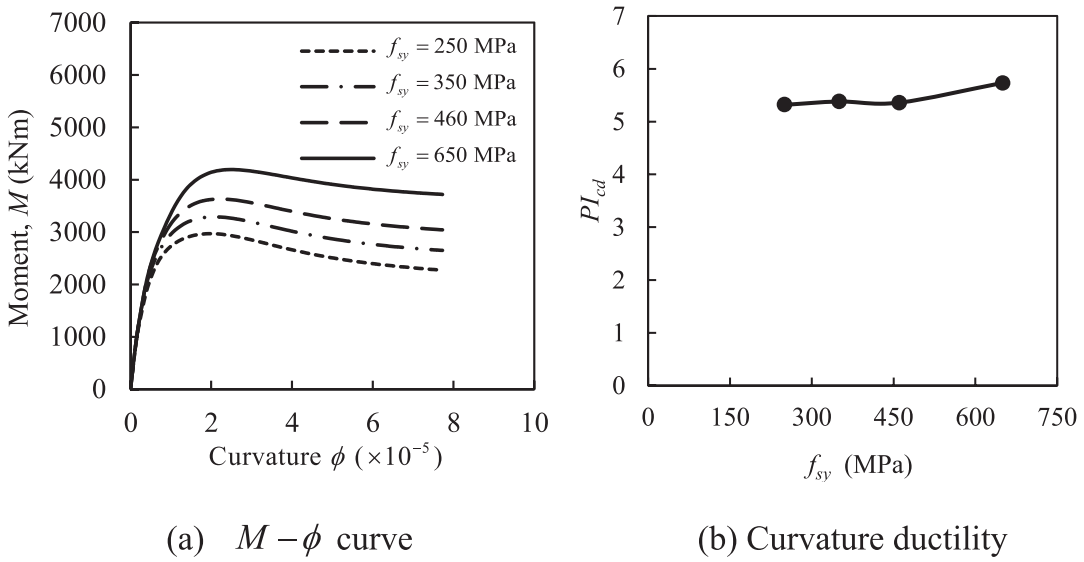

FIGURE 14 Influences of steel yield stress on the performance of OCFST beam-columns. (a) $M-\phi$ curves. (b) Curvature ductility. OCFST, octagonal concrete-filled steel tubular.

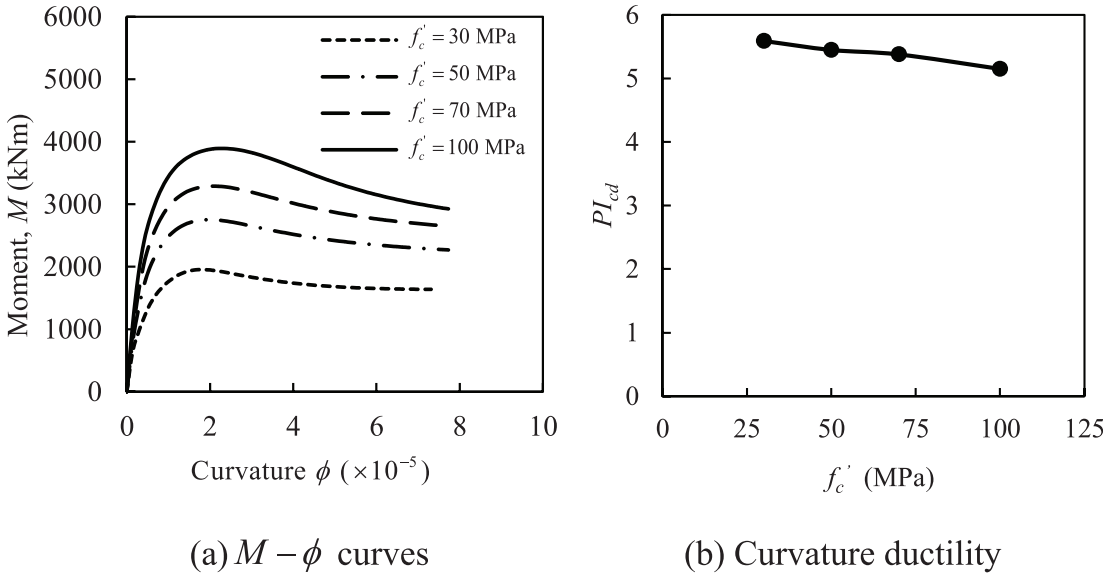

FIGURE 16 Influences of concrete strength on the performance of OCFST beam-columns. (a) $M-\phi$ curves. (b) Curvature ductility. OCFST, octagonal concrete-filled steel tubular.

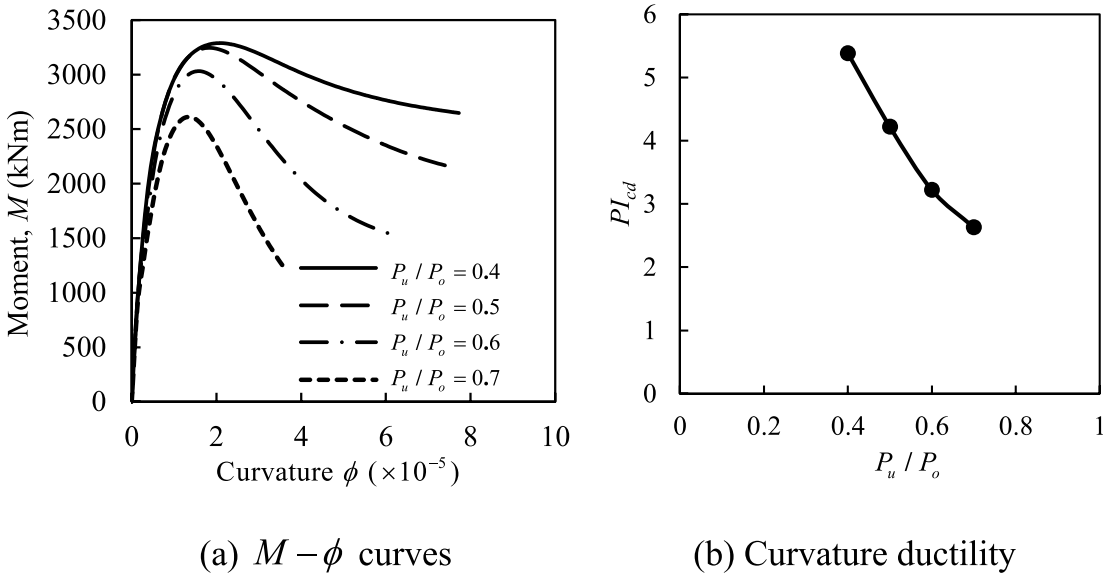

FIGURE 17 Influences of P_u/P_o ratio on the behavior of OCFST columns. (a) $M-\phi$ curves. (b) Curvature ductility. OCFST, octagonal concrete-filled steel tubular.

in which P_u and P_o stand for the eccentric load and the pure ultimate axial load of the columns, respectively, and M_u and M_o represent the bending moment and pure bending moment of the columns, respectively. The P_o and M_o are to be calculated as

$$P_{o,AISC} = A_s f_{sy} + 0.95 A_c f'_c, \quad (15)$$

$$M_o = (W_{ps} - W_{psn}) f_{sy} + 0.5(W_{pc} - W_{pcn}) 0.95 f'_c, \quad (16)$$

where W_{ps} and W_{pc} are the plastic modulus of steel tube and concrete, respectively; W_{psn} and W_{pcn} denote the plastic modulus of steel tube and concrete within $2h_n$, respectively; h_n denotes the distance from the neutral axis to the centroid of the cross-section; A_s and A_c represent the areas of steel tube and concrete, respectively.

6.2 | Proposed interaction equations

Based on the numerical results obtained in this study, interaction equations for expressing the interaction curve of OCFST short columns are proposed herein as

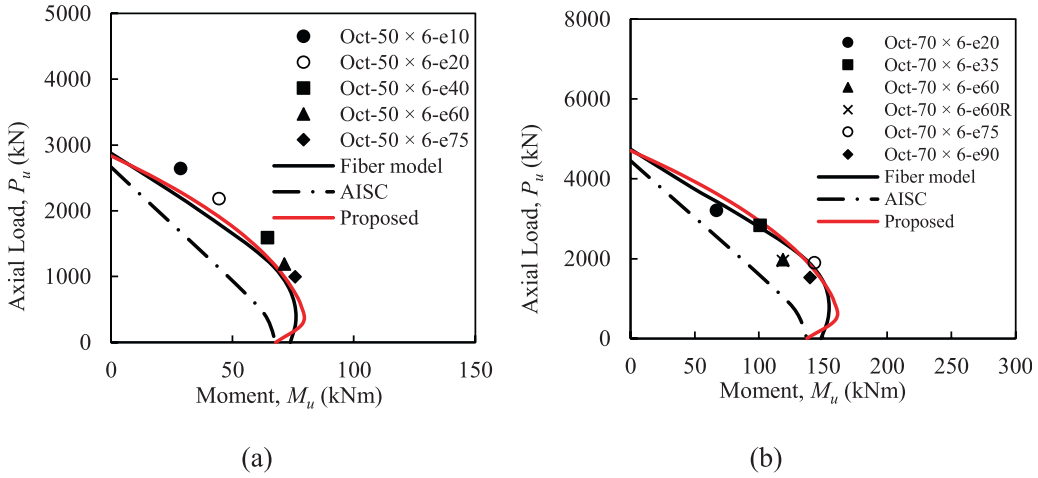

FIGURE 18 Comparison of the proposed $P_u - M_u$ curves of OCFST columns with the test results. OCFST, octagonal concrete-filled steel tubular.

FIGURE 19 Comparisons of the proposed $P_u - M_u$ curves of OCFST columns with ones obtained from the numerical analysis. (a) D/t ratio by changing the external diameter; (b) D/t ratio by changing steel tube thickness; (c) concrete strength; (d) steel yield stress. OCFST, octagonal concrete-filled steel tubular.

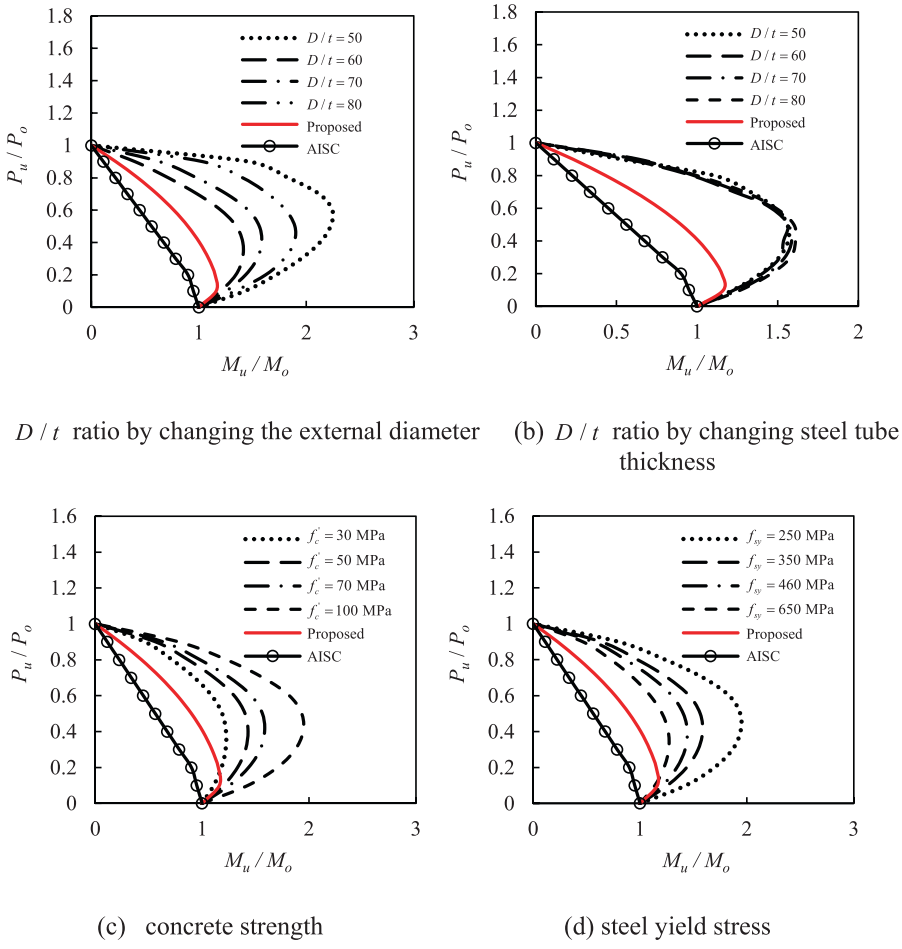

$$M_u = 1.2M_o\left[1-\left(\frac{P_u}{P_o}\right)^2\right] \quad \text{for} \quad P_u \geq 0.2P_o, \qquad (17)$$

$$M_u = M_o\left[1+\frac{1}{5}\left(\frac{P_u}{P_o}\right)^{0.09}\right] \quad \text{for} \quad P_u < 0.2P_o, \qquad (18)$$

where M_o is calculated using Equation (16) and P_o is given by Ahmed and Liang[20] as

$$P_{o,prop} = A_s f_{sy} + \left(\gamma_c f'_c + 4.1 f_{rp}\right) A_c, \quad (19)$$

where f_{rp} is given in Equation (9).

6.3 | Accuracy of the proposed interaction equations

The accuracy of the proposed interaction equations for OCFST short beam-columns as well as the one specified in AISC 360-16 for CFST columns is examined by comparison with the test results of Fang et al.[17] in Figure 18 and numerical results in Figure 19. As shown, the proposed design equations can provide a more accurate prediction of the P_u-M_u curves of OCFST columns than the one given in AISC 360-16. This is because AISC 360-16 does not consider the confinement provided by OCFST steel tube to the core concrete so that it underestimates the ultimate strength of the columns. On the contrary, the material constitutive model for concrete in OCFST columns utilized in this study considers the confinement effect on the core concrete. Therefore, in the absence of the design specifications for the P_u-M_u curves of OCFST columns, the proposed interaction equations can be used for design purposes. However, the proposed model seems to provide conservative strength predictions of the Oct-50×6 series having a small eccentricity. However, the proposed model captures well the strengths of the Oct-70×6 series. The difference is likely due to the uncertainty in the concrete strength of the actual tested columns as the average compressive strength was used in the analysis.

7 | CONCLUSIONS

A computationally efficient numerical model of fiber analysis has been developed and presented in this paper for the simulation of the nonlinear inelastic behavior of OCFST short beam-columns subjected to eccentric loads. The method of analysis accounts for the distributed plasticity of octagonal steel tube, concrete cracking and crushing, and confinement effects. The computational procedures have been described that compute the load–moment interaction diagrams and moment–curvature curves. The numerical results obtained were compared with test results reported elsewhere. It has been shown that the strengths of eccentrically loaded OCFST short beam-columns can be predicted by the proposed analysis method with good accuracy. The validated model has been used to study the influences of various parameters on the P_u-M_u curves, the $M-\phi$ curves, and the curvature ductility of high-strength OCFST short beam-columns. For practical purposes, interaction equations for expressing the axial load–moment strength envelopes of OCFST short beam-columns have been proposed.

The important outcomes obtained from the study are as follows:

a. Increasing the D/t ratio by changing the steel tube thickness considerably reduces the stiffness, bending strengths, and curvature ductility of OCFST short beam-columns. On the other hand, the stiffness, bending strengths, and ductility increase significantly as D/t ratio increases by varying the diameter and keeping the same thickness.
b. Increasing the steel yield strength significantly improves the bending capacity of OCFST columns. However, steel yield strength has insignificant effects on the curvature ductility of the columns.
c. For the identical cross-section, concrete strength has the most significant effect on the performance of OCFST short beam-columns. The use of high-strength concrete in OCFST short beam-columns improves their bending strengths but decreases their curvature ductility.
d. An increase in the axial load level significantly reduces the ultimate bending strength and curvature ductility of OCFST beam-columns.
e. The proposed formulas predict the P_u-M_u curves of OCFST beam-columns more accurately than the interaction equations specified in AISC 360-16.

ACKNOWLEDGMENTS

Open access publishing facilitated by Victoria University, as part of the Wiley - Victoria University agreement via the Council of Australian University Librarians.

DATA AVAILABILITY STATEMENT

The data that support the findings of this study are available from the corresponding author upon reasonable request.

ORCID

Qing Quan Liang https://orcid.org/0000-0003-0333-2265

REFERENCES

1. Han L-H, Li W, Bjorhovde R. Developments and advanced applications of concrete-filled steel tubular (CFST) structures: members. J Constr Steel Res. 2014;100:211–28.
2. Patel VI, Liang QQ, Hadi MNS. Nonlinear analysis of concrete-filled steel tubular columns. Germany: Scholar's Press; 2015.

3. Hou C-C, Han L-H. Life-cycle performance of deteriorated concrete-filled steel tubular (CFST) structures subject to lateral impact. Thin-Walled Struct. 2018;132:362–74.
4. Sakino K, Nakahara H, Morino S, Nishiyama I. Behavior of centrally loaded concrete-filled steel-tube short columns. J Struct Eng. 2004;130(2):180–8.
5. Uy B. Strength of short concrete filled high strength steel box columns. J Constr Steel Res. 2001;57(2):113–34.
6. Han LH. Flexural behaviour of concrete-filled steel tubes. J Constr Steel Res. 2004;60(2):313–37.
7. Liang QQ. Performance-based analysis of concrete-filled steel tubular beam–columns, part I: theory and algorithms. J Constr Steel Res. 2009;65(2):363–72.
8. Patel VI, Liang QQ, Hadi MNS. High strength thin-walled rectangular concrete-filled steel tubular slender beam-columns, part I: modeling. J Constr Steel Res. 2012;70:377–84.
9. Katwal U, Tao Z, Hassan MK, Wang WD. Simplified numerical modeling of axially loaded circular concrete-filled steel stub columns. J Struct Eng. 2017;143(12):04017169.
10. Xiong MX, Xiong DX, Liew JYR. Axial performance of short concrete filled steel tubes with high- and ultra-high-strength materials. Eng Struct. 2017;136:494–510.
11. Tomii M, Yoshimura K, Morishita Y. Experimental studies on concrete-filled steel tubular stub columns under concentric loading. International colloquium on stability of structures under static and dynamic loads. New York: ASCE; 1977. p. 718–41.
12. Evirgen B, Tuncan A, Taskin K. Structural behavior of concrete filled steel tubular sections (CFT/CFSt) under axial compression. Thin-Walled Struct. 2014;80:46–56.
13. Ding F-X, Li Z, Cheng S, Yu Z-W. Composite action of octagonal concrete-filled steel tubular stub columns under axial loading. Thin-Walled Struct. 2016;107:453–61.
14. Zhu J-Y, Chan T-M. Behaviour of polygonal-shaped steel-tube columns filled with high-strength concrete. ICE Proceedings Structures and Buildings. 2017;171(2):96–112.
15. Zhu J-Y, Chan T-M. Experimental investigation on octagonal concrete filled steel stub columns under uniaxial compression. J Constr Steel Res. 2018;147:457–67.
16. Zhu J-Y, Chan T-M. Experimental investigation on steel-tube-confined-concrete stub column with different cross-section shapes under uniaxial-compression. J Constr Steel Res. 2019;162:105729.
17. Fang H, Li Q-Y, Chan T-M, Young B. Behaviour and design of high-strength octagonal CFST short columns subjected to combined compression and bending. J Constr Steel Res. 2023;200:107679.
18. Susantha KAS, Ge H, Usami T. Uniaxial stress–strain relationship of concrete confined by various shaped steel tubes. Eng Struct. 2001;23(10):1331–47.
19. Hassanein MF, Patel VI, Elchalakani M, Thai H-T. Finite element analysis of large diameter high strength octagonal CFST short columns. Thin-Walled Struct. 2018;123:467–82.
20. Ahmed M, Liang QQ. Numerical modeling of octagonal concrete-filled steel tubular short columns accounting for confinement effects. Eng Struct. 2020;226:111405.
21. Eurocode 4. Design of composite steel and concrete structures – Part 1-1: general rules and rules for buildings. Brussels, Belgium: European Committee for Standardization (CEN); 2004.
22. AISC 360-16. Specification for structural steel buildings. Chicago (IL), USA: American Institute of Steel Construction; 2016.
23. AS 3600-2009. Concrete structures. Sydney, NSW, Australia: Standards Australia; 2009.
24. Ahmed M, Liang QQ, Patel VI, Hadi MNS. Nonlinear analysis of rectangular concrete-filled double steel tubular short columns incorporating local buckling. Eng Struct. 2018;175:13–26.
25. Liang QQ. Nonlinear analysis of circular double-skin concrete-filled steel tubular columns under axial compression. Eng Struct. 2017;131:639–50.
26. Ahmed M, Sheikh MN, Hadi MN, Liang QQ. Numerical simulation of axially loaded square high-strength concrete short columns with steel equal-angles as longitudinal reinforcement. Eng Struct. 2023;276:115391.
27. Persson PO, Strang G. A simple mesh generator in MATLAB. SIAM Rev. 2004;46(2):329–45.
28. Lai ZC, Varma AH. Effective stress-strain relationships for analysis of noncompact and slender filled composite (CFT) members. Eng Struct. 2016;124:457–72.
29. Lin S, Zhao Y-G, Lu Z-H. Fibre beam element models for nonlinear analysis of concentrically loaded circular CFT columns considering the size effect. Eng Struct. 2020;210:110400.
30. El-Tawil S, Deierlein GG. Strength and ductility of concrete encased composite columns. J Struct Eng. 1999;125(9):1009–19.
31. Ahmed M, Liang QQ, Patel VI, Hadi MNS. Experimental and numerical studies of square concrete-filled double steel tubular short columns under eccentric loading. Eng Struct. 2019;197:109419.
32. Ahmed M, Liang QQ, Patel VI, Hadi MNS. Local-global interaction buckling of square high-strength concrete-filled double steel tubular slender beam-columns. Thin-Walled Struct. 2019;143:106244.
33. Mander JB. Seismic design of bridge piers. Christchurch, New Zealand: Department of Civil Engineering, University of Canterbury; 1983 Ph.D. Thesis.
34. Lim JC, Ozbakkaloglu T. Stress–strain model for normal- and light-weight concretes under uniaxial and triaxial compression. Constr Build Mater. 2014;71:492–509.
35. Popovics S. A numerical approach to the complete stress-strain curve of concrete. Cem Concr Res. 1973;3(5):583–99.
36. De Nicolo B, Pani L, Pozzo E. Strain of concrete at peak compressive stress for a wide range of compressive strengths. Mater Struct. 1994;27(4):206–10.
37. Mander JB, Priestley MJN, Park R. Theoretical stress-strain model for confined concrete. J Struct Eng. 1988;114(8):1804–26.
38. Richart FE, Brandtzaeg A, Brown RL. A study of the failure of concrete under combined compressive stresses. Illinois: Engineering Experiment Station, College of Engineering, University of Illinois, Champaign; 1928.
39. Ahmed M, Liang QQ, Patel VI, Hadi MNS. Computational simulation of eccentrically loaded circular thin-walled concrete-filled double steel tubular slender columns. Eng Struct. 2020;213:110571.
40. Ahmed M, Liang QQ, Patel VI, Hadi MNS. Behavior of eccentrically loaded double circular steel tubular short columns filled with concrete. Eng Struct. 2019;201:109790.
41. Liang QQ, Fragomeni S. Nonlinear analysis of circular concrete-filled steel tubular short columns under eccentric loading. J Constr Steel Res. 2010;66(2):159–69.

AUTHOR BIOGRAPHIES

Mizan Ahmed, Centre for Infrastructure Monitoring and Protection, School of Civil and Mechanical Engineering, Curtin University, Kent Street, Bentley, WA 6102, Australia.
Email: mizan.ahmed@curtin.edu.au

Qing Quan Liang, College of Sport, Health, and Engineering, Victoria University, PO Box 14428, Melbourne, VIC 8001, Australia.
Email: qing.liang@vu.edu.au

Vipulkumar Ishvarbhai Patel, School of Computing, Engineering and Mathematical Sciences, La Trobe University, Bendigo, VIC 3552, Australia.
Email: v.patel@latrobe.edu.au

Ahmed Hamoda, Civil Engineering Department, Faculty of Engineering, Kafrelsheikh University, Kafrelsheikh, Egypt.
Email: ahmed_hamoda@eng.kfs.edu.eg

How to cite this article: Ahmed M, Liang QQ, Patel VI, Hamoda A. Inelastic analysis of octagonal concrete-filled steel tubular short columns under eccentric loading. Structural Concrete. 2023. https://doi.org/10.1002/suco.202300360